Article

Significant Influence of a Single Atom Change in Auxiliary Acceptor on Photovoltaic Properties of Porphyrin-Based Dye-Sensitized Solar Cells

Haoran Zhou, Jung-Min Ji, Min Su Kim and Hwan Kyu Kim *

Global GET-Future Laboratory & Department of Advanced Materials Chemistry, Korea University,
2511 Sejong-ro, Sejong 339-700, Korea; zhouhaoran@naver.com (H.Z.); manbbong@korea.ac.kr (J.-M.J.);
kimms38@korea.ac.kr (M.S.K.)
* Correspondence: hkk777@korea.ac.kr; Tel.: +82-44-860-1493

check for updates

Abstract: The rational design of porphyrin sensitizers is always crucial for dye-sensitized solar cells (DSSCs), since the change of only a single atom can have a significant influence on the photovoltaic performance. We incorporated the pyridothiadiazole group, as a stronger electron-withdrawing group, into the commonly well-established skeleton of D-porphyrin-triple bond-acceptor sensitizers by a single atom change for a well-known strong electron-withdrawing benzothiadiazole (BTD) unit as an auxiliary acceptor. The impact of the pyridothiadiazole group on the optical; electrochemical; and photovoltaic properties of D–π–A porphyrin sensitizers was investigated with comparison for a benzothiadiazole-substituted **SGT-020** porphyrin. The pyridothiadiazole-substituted **SGT-024** porphyrin dye was red-shifted so that the absorption range might be expected to achieve higher light harvest efficiency (LHE) than the **SGT-020** porphyrin. However, all the devices were fabricated by utilizing **SGT-020** and **SGT-024**, evaluated and found to achieve a cell efficiency of 10.3% for **SGT-020**-based DSSC but 4.2% for **SGT-024**-based DSSC under standard global AM 1.5G solar light conditions. The main reason is the lower charge collection efficiency of **SGT-024**-based DSSC than **SGT-020**-based DSSC, which can be attributed to the tilted dye adsorption mode on the TiO$_2$ photoanode. This may allow for faster charge recombination, which eventually leads to lower J_{sc}, V_{oc} and power conversion efficiency (PCE).

Keywords: D–π–A structural porphyrin; acceptor units; dye-sensitized solar cells; charge recombination; charge collection efficiency

1. Introduction

A huge amount of work has recently concentrated on third-generation solar cell technology development with low cost as emerging photovoltaics, such as dye-sensitized solar cells (DSSCs) [1,2], organic photovoltaics (OPVs) [3–5], perovskite solar cells (PSCs) [6–8], etc. Among the various solar technologies, DSSCs have garnered considerable attention due to the simple fabrication process, low cost, low toxicity, and high PCE under ambient lighting conditions [9,10]. In 1991 Grätzel and O'Regan first introduced mesoporous TiO$_2$ nanocrystal layers into the DSSC system [11]. This led to a substantial improvement in photoelectric transformation efficiency. Since then, over the past 28 years, DSSCs have continued to show improved PCE [12–14]. Until now, state-of-the-art DSSCs have achieved PCEs approaching >11.9% for ruthenium complexes [15], >14% for metal-free D–π–A structural organic sensitizers [16], and 14.64% for D–π–A structural organic sensitizer-based tandem DSSCs under standard (1.5) illumination [13]. In comparison with ruthenium sensitizers [17,18] and metal-free sensitizers [19,20], D–π–A structural porphyrin sensitizers [21–23] have been attractive

due to their extremely high molar extinction coefficient, exceptional ability to harvest light, and high photostability. To date, porphyrin-based DSSCs have achieved PCE by more than 13% under standard (1.5) illumination [24,25].

However, there are also some drawbacks due to the nature of porphyrins, such as the weak absorption in the range of 500–600 nm, the lack of absorption in the near-infrared region (NIR), and the dye aggregation caused by the extended π-conjugation structure [26–30]. It is apparent that these problems could be overcome by rational structural optimization. For example, long and well-adjusted alkoxy chains were introduced to porphyrin molecules, which significantly diminished the dye aggregation and reduced the interface back electron transfer rate [31]. The introduction of a benzothiadiazole (BTD) unit in the acceptor part to the well-established platform of D-porphyrin-triple bond-acceptor sensitizers was also a promising approach for elevating light-harvesting properties, as well as the photovoltaic performance. Up to now, the BTD unit was one of the most commonly used auxiliary electron acceptors in the well-known skeleton of D-porphyrin-triple bond-BTD-acceptor sensitizers for DSSCs [32–34].

In order to reduce the HOMO (highest occupied molecular orbital)–LUMO (lowest unoccupied molecular orbital) energy gap as well as extend the absorption range, a boosted electron-withdrawing pyridothiadiazole unit was introduced into the well-established platform of D-porphyrin-triple bond-BTD-acceptor sensitizers by a single atom change for the well-known strong electron-withdrawing benzothiadiazole (BTD) unit as an auxiliary acceptor. Although the pyridothiadiazole unit has been widely used in D–A polymers in OPVs [35,36] and metal-free organic sensitized solar cells [37,38], no application of the pyridothiadiazole unit has been explored in porphyrin-sensitized solar cells. Thus, based on our previously reported dye of **SGT-020 [25]**, we expected that the pyridothiadiazole unit in D–π–A porphyrin sensitizers could improve the absorption ability in NIR as well as the light harvest efficiency. Thus, a novel D–π–A structural porphyrin sensitizer was designed and synthesized, named as **SGT-024**, as shown in Scheme 1. Meanwhile, the optical properties, electrochemical properties, and photovoltaic performances were systemically investigated.
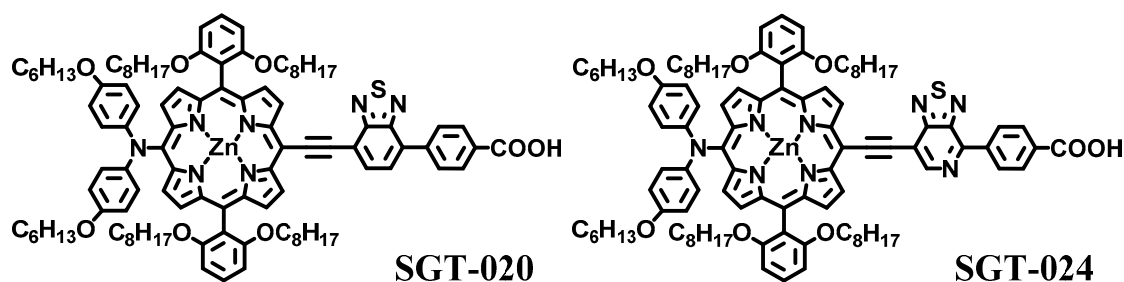
Scheme 1. Molecular structures of **SGT-020** and **SGT-024** sensitizers.

2. Synthetic Procedure

All reagents were purchased from Alfa Aesar (Haverhill, MA, USA), TCI (Tokyo, Japan), and Sigma–Aldrich (St. Louis, MO, USA) unless stated otherwise. The synthesis routes of **SGT-024** were shown in Scheme 2, and compound **1** [37], compound **3** [25], and **SGT-020** [25] were synthesized according to the respective literature procedures. Details on the synthetic procedure, instrumentation, DSSC fabrication, photovoltaic parameters, ^{1}H-NMR, ^{13}C-NMR, and MALDI-TOF data are given in the Supplementary Materials.
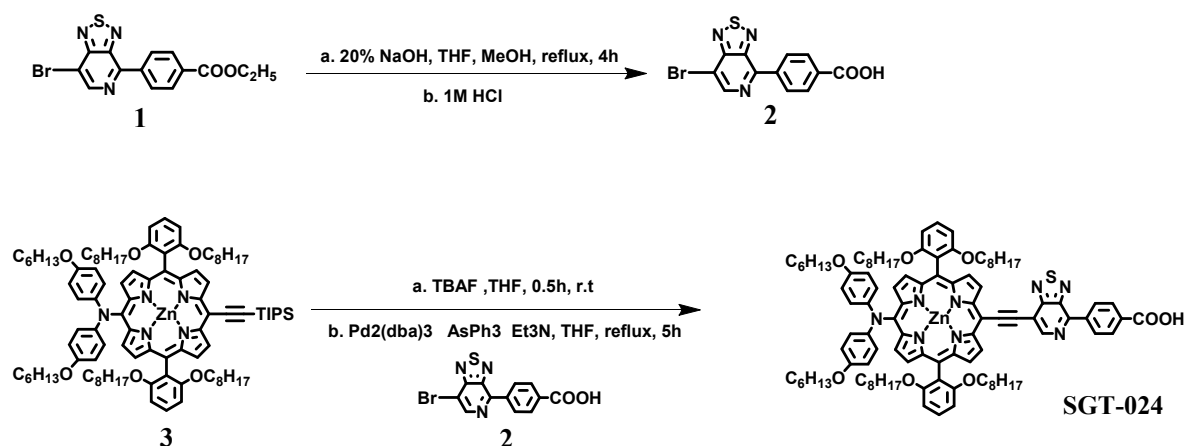
Scheme 2. Synthesis routes of **SGT-024**.

3. Results and Discussion

The UV-visible spectra of the dyes **SGT-020** and **SGT-024** in THF were collected and reported in Figure 1. It is obvious that **SGT-020** and **SGT-024** showed two intense absorption regions within the ranges of 400 to 500 nm (Soret band) and 600 to 800 nm (Q band). In Table 1, compared with the molar extinction coefficient (ε) of 143,040 M^{-1} cm^{-1} at the maximum absorption wavelength (λ_{max} = 454 nm) observed for **SGT-020**, the λ_{max} of **SGT-024** is 430 nm with a coefficient of 123,162 M^{-1} cm^{-1}. It should be noted that the Soret band peaks of **SGT-024** were blue-shifted but the Q bands were significantly red-shifted when a pyridothiadiazole unit was introduced into the platform of D-porphyrin-triple bond-acceptor sensitizers by a single atom change for the well-known strong electron-withdrawing benzothiadiazole (BTD) unit. Furthermore, the fluorescent emission spectra were also measured in THF, as shown in Figure 1. **SGT-020** and **SGT-024** exhibited major emission bands at 724 and 791 nm, respectively. Therefore, the optical properties of these two porphyrin sensitizers revealed that the light capture region could be expanded by introducing the stronger electron-withdrawing moiety of the pyridothiadiazole unit.
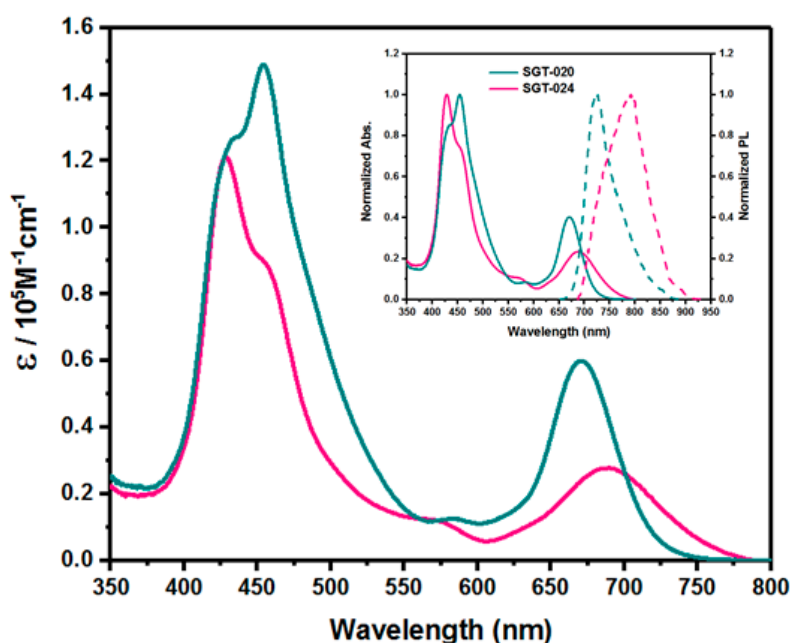
Figure 1. Absorption spectra and emission spectra of **SGT-020** and **SGT-024** in THF.

The electrochemical properties of **SGT-020** and **SGT-024** were evaluated in THF with 0.1 M TBAPF$_6$ as an electrolyte, using cyclic voltammetry (CV) (see Figure S2); the corresponding data are collected in Table 1. As shown in Figure 2, due to the fact that they have the same donor unit, their ground state oxidation potentials, which correspond to the HOMO energy levels of **SGT-020** and **SGT-024**, are nearly the same. Meanwhile, from the HOMO–LUMO band gap and the oxidation potential, the reduction potentials of **SGT-020** and **SGT-024** were determined to be −0.93 and −0.81 eV, respectively. This difference in reduction potentials could be ascribed to the structural changes in the acceptor group. The results also revealed that the reduction potential values are much more negative than the conducting band (CB) of TiO$_2$ and the oxidation potential values are much more positive than the Co(bpy)$_3^{2+/3+}$ (bpy = 2,2′-bipyridine) redox couple (0.56 V vs. NHE), indicating that all of the electron transfer processes for two porphyrin sensitizers should occur efficiently due to the sufficient driving force.
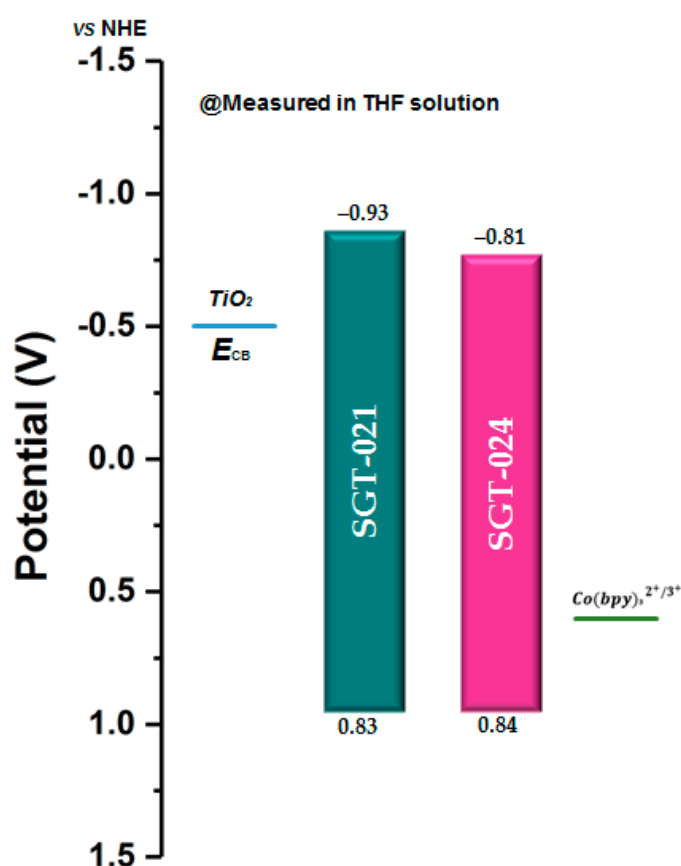

Figure 2. Energy-level diagram of **SGT-020** and **SGT-024**.

Table 1. Photophysical and electrochemical data for **SGT-020** and **SGT-024**.

Dye	$\lambda_{abs\,max}$ [a] (nm)	ε (M^{-1} cm^{-1})	$\lambda_{em\,max}$ [a] (nm)	E_{0-0} [b] (eV)	S^+/S [c] (eV) [V vs. NHE]	S^+/S^* [d] (eV) [V vs. NHE]
SGT-020	454 670	143,040 59,916	724	1.73	0.83	−0.93
SGT-024	430 687	123,162 27790	791	1.65	0.84	−0.81

[a] Absorption and emission spectra were measured in THF. [b] E_{0-0} was determined from the intersection of normalized absorption and emission spectra in THF. [c] Oxidation potentials of dyes were measured in THF with 0.1 M TBAPF$_6$, ferrocene/ferrocenium internal reference. [d] Excited-state oxidation potentials were calculated according to $(S^+/S$ [c]$) - E_{0-0}$.

DFT calculations at the M06 [39]/6-31G [40] (LANL2DZ [41] for Zn atom) level were carried out to better understand the electron distribution and the molecular geometries. The optimized ground state molecular structures and dihedral angles (between BTD/pyridothiadiazole unit and benzoic acid) of two porphyrins are shown in Figure 3 and Table S1. The electron distribution of the HOMO energy levels was mainly delocalized at the diphenylamine donor unit and porphyrin core. However, as for the electron distribution of the LUMO energy levels, **SGT-024** showed a more evident shift to the unit of benzoic acid than **SGT-020**. Thus, **SGT-024** was expected to show enhanced intramolecular charge transfer (ICT) compared to that of **SGT-020**. Furthermore, in the optimized structures of **SGT-020** and **SGT-024**, the dihedral angles between the adjacent auxiliary acceptor and benzoic acid are 35.02° and 16.06°, respectively. Therefore, owing to the significant reduction of the torsion angle, **SGT-024** displayed more efficient π-conjugation and a better coplanar geometry in comparison with **SGT-020**, but this geometry would increase the possibility of dye aggregation.
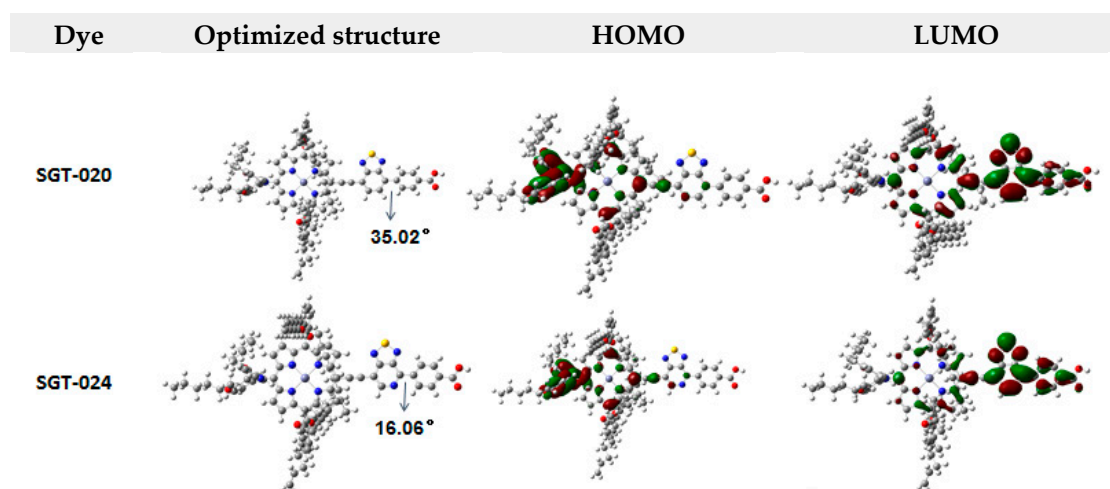

Dye	Optimized structure	HOMO	LUMO
SGT-020	35.02°		
SGT-024	16.06°		

Figure 3. Optimized molecular geometries and electron distributions of the HOMO and LUMO energy levels of **SGT-020** and **SGT-024**.

The photovoltaic characteristics of the **SGT-020**- and **SGT-024**-based devices were measured under standard AM 1.5 conditions. The porphyrin-based TiO$_2$ films were used as the photoanode in DSSCs, employing the Co(bpy)$_3$$^{2+/3+}$ redox couple as electrolyte and CDCA (chenodeoxycholic acid) as co-adsorbent. The relevant photocurrent density-voltage (J-V) curves are shown in Figure 4a and the device parameters are summarized in Table 2. As compared to the reference dye **SGT-020** (J_{sc} = 14.8 mA cm^{-2}, V_{oc} = 0.806 V, FF = 73.2% and PCE = 8.7%), the pyridothiadiazole-incorporated dye **SGT-024** only showed a moderate PCE of only 1.7%. The J_{sc} value of **SGT-024** dramatically dropped to 3.3 mA cm^{-2} and its V_{oc} also decreased to 0.655 V. To further investigate the J_{sc} value of each porphyrin sensitizer, the corresponding IPCE (incident photon-to-electron conversion efficiency) spectra of **SGT-020** and **SGT-024**-based devices were measured under AM 1.5G solar light. As shown in Figure 4b, **SGT-024** sensitizers exhibited a broader, weaker absorption response (the absorption onset extended to almost 900 nm) than **SGT-020** (to ~850 nm), which displayed a similar tendency with the absorption spectra on TiO$_2$ film, as shown in Figure S1. On the contrary, the **SGT-024**-based DSSCs exhibited an extremely low IPCE value (no more than 20% from 400 to 900 nm; thus, lower J_{sc} values were observed.
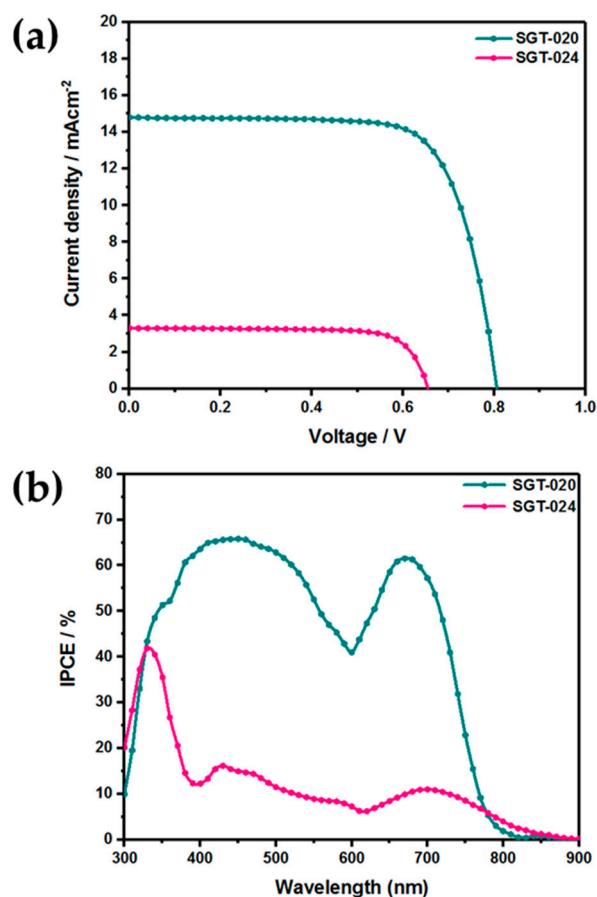
Figure 4. (**a**) Current-voltage characteristics of the **SGT-020** and **SGT-024**-based DSSCs and (**b**) the corresponding IPCE spectra under 100 mW cm^{-2} simulated AM 1.5G solar light.

Table 2. Photovoltaic parameters of the **SGT-020** and **SGT-024**-based DSSCs under 100 mW cm^{-2} simulated AM 1.5G solar light.

Dye	Co-Adsorbent	Adsorption Amount (10^{-8} mol cm^{-2})	J_{sc} (mA cm^{-2})	V_{oc} (mV)	*FF* (%)	PCE [a] (%)
SGT-020	CDCA	2.13	14.8 ± 0.53	806 ± 9.8	73.2 ± 2.4	8.7 ± 0.25
SGT-024		1.95	3.3 ± 0.25	655 ± 7.3	76.3 ± 1.7	1.7 ± 0.15
SGT-020	HC-A1	1.87	16.9 ± 0.32	795 ± 8.5	76.8 ± 2.1	10.3 ± 0.12
SGT-024		1.79	7.3 ± 0.12	724 ± 6.7	79.0 ± 1.8	4.2 ± 0.19

In order to further improve the photovoltaic performance of **SGT-020** and **SGT-024**-based DSSCs, another co-adsorbent called **HC-A1** was introduced in this study. **HC-A1**, a multi-functional co-adsorbent widely used in our previous research [13,42], and its structure are shown in Figure S3. As expected, because of the light harvesting in shorter wavelength regions and efficient charge recombination retardation [43–46], the PCE of **SGT-020** and **SGT-024**-based solar cells was dramatically improved to 10.3% and 4.2%, respectively (see Figure 5). In addition, the dye loading amounts for **SGT-020** and **SGT-024** were found to be almost no different, implying that the effect of the dye loading amount on photovoltaic performance in this study is relatively small.
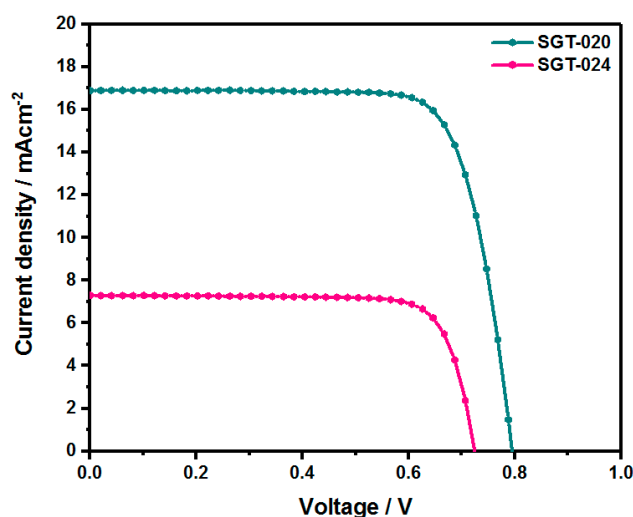
Figure 5. Current-voltage characteristics of the **SGT-020** and **SGT-024**-based DSSCs with **HC-A1** under 100 mW cm^{-2} simulated AM 1.5G solar light.

In order to get deeper insight into the photovoltaic performance difference as well as the interfacial charge transfer in all DSSC devices, the electrochemical impedance spectroscopy (EIS) was measured in the dark. Nyquist plots and Bode plots are shown in Figure 6 (a) and (b), respectively, and the EIS data are collected in Table 3. As far as we know, the first, second, and third semicircles correspond to the charge transfer resistance at the counter electrode, the resistance of TiO$_2$/dye/electrolyte interface, and the diffusion resistance of Co(bpy)$_3{}^{2+/3+}$ redox couple in the electrolyte, respectively. The second semicircle of **SGT-024** (R_{rec} = 6.12) was found to be much smaller than **SGT-020** (R_{rec} = 16.8), indicating that the electron recombination rate of **SGT-024** is higher than that of **SGT-020**. On the other hand, according to the equation $\tau_r = C_\mu \cdot R_{rec}$, the electron lifetime was calculated to be 5.12 or 3.33 ms for **SGT-020** and **SGT-024**, respectively. Meanwhile, the charge-collection efficiency η_{cc}, derived from $\eta_{cc} = (1 + R_{tr}/R_{rec})^{-1}$ [47], was confirmed to be 84% for **SGT-020** and 68% for **SGT-024**. The results obtained above are consistent with the V_{oc} values for the **SGT-020**-based device (0.795 V) and **SGT-024**-based device (0.724 V). Thus, when compared to **SGT-020** and **SGT-024**, the higher charge recombination rate and the lower charge collection efficiency of the **SGT-024**-based device may be the main reasons for its disappointing lower photovoltaic performance.
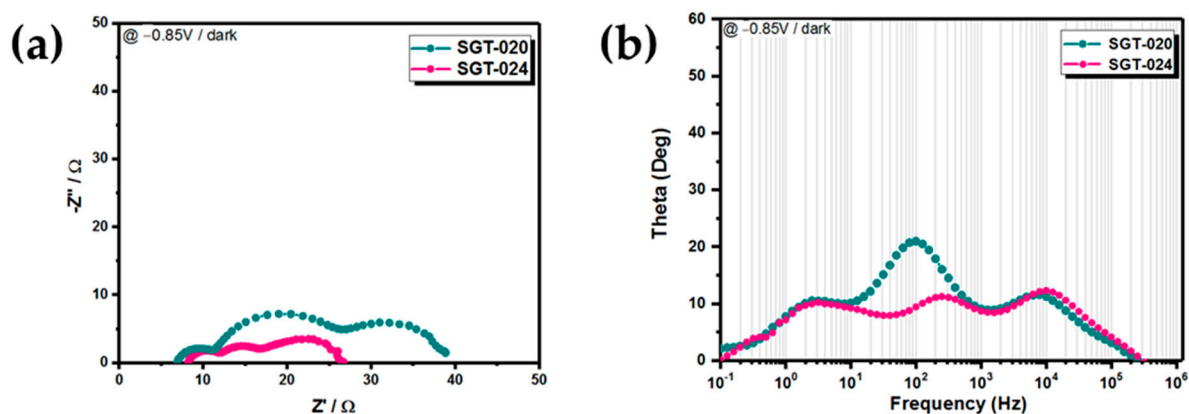

Figure 6. Nyquist plots (**a**) and Bode phase plots (**b**) based on **SGT-020** and **SGT-024** under dark.

Table 3. EIS data for the **SGT-020**- and **SGT-024**-based DSSCs.

Device [a]	EIS [b]					
	R_{tr} (Ω)	R_{rec} (Ω)	C_μ (mF)	τ_n (ms)	τ_r (ms)	η_{cc} (%)
SGT-020	3.27	16.8	0.30	0.99	5.12	84
SGT-024	2.85	6.12	0.54	1.55	3.33	68

[a] DSSCs were fabricated with **HC-A1**. [b] forward bias of 0.85 V under dark conditions. R_{tr}: transport resistance; R_{rec}: charge recombination resistance; C_μ: chemical capacitance; τ_n: transport time; τ_r: electron lifetime; η_{cc}: charge collection efficiency.

4. Conclusions

In this work, in order to investigate the structure-performance relationship between the photovoltaic performance and the structure of various acceptors, the pyridothiadiazole group, as a stronger electron-withdrawing group, was incorporated into the well-established skeleton of D-porphyrin-triple bond-acceptor sensitizers by a single atom change for the well-known strong electron-withdrawing benzothiadiazole (BTD) unit. The impact of the pyridothiadiazole group on the optical, electrochemical, and photovoltaic properties of D–π–A porphyrin sensitizers was investigated by comparing with a benzothiadiazole-substituted **SGT-020** porphyrin. The porphyrin **SGT-024** presents a red-shifted and broadened Q-band in comparison with **SGT-020**, which could be attributed to the stronger electron-withdrawing nature of pyridothiadiazole than the **BTD** unit. This revealed that the introduction of pyridothiadiazole would be an effective strategy for strengthening the absorption of the well-established skeleton of D-porphyrin-triple bond-acceptor sensitizers, although it shows a more moderate PCE of 4.2% than the DSSC based on **SGT-020** (10.3%). The serious efficiency loss for the **SGT-024**-based device could be for two main reasons: the fast charge recombination rate caused by the strong electron-withdrawing acceptor, and thus lower charge collection efficiency observed; and the enhanced backbone co-planarity in **SGT-024** leading to unexpected dye aggregation. However, the pyridothiadiazole unit is still a promising synthetic strategy to explore D–π–A structural porphyrins with extended absorption properties. Our study has underlined the importance of a suitable auxiliary acceptor between the dye and the anchoring group for a sensitizer. This should be seriously considered in the further rational design of dye-sensitized solar cells.

Supplementary Materials: The following are available online at http://www.mdpi.com/2079-4991/8/12/1030/s1. Informative details of material synthesis and characterization, DSSC fabrication, and photoelectrochemical measurements are available in the Supplementary Materials. Figure S1: UV spectra of the porphyrin sensitizers on a TiO$_2$ film (3 μm), Figure S2: Cyclic voltammograms of **SGT-020** and **SGT-024** in THF/ TBAPF$_6$ and ferrocene external reference, Figure S3: Co-adsorbents used in the dye-sensitized solar cells, Figure S4: ^{1}H-NMR spectrum (300 MHz, (CD$_3$)$_2$CO) of SGT-024, Figure S5: ^{13}C-NMR spectrum (300 MHz, (CD$_3$)$_2$CO) of **SGT-024**, Figure S6: Maldi-TOF spectrum of **SGT-024**, Table S1: Photophysical and electrochemical properties of porphyrin sensitizers by DFT calculations.

Conflicts of Interest: The authors declare no conflict of interest.

References

1. Ji, J.-M.; Zhou, H.; Kim, H.K. Rational design criteria for D–π–A structured organic and porphyrin sensitizers for highly efficient dye-sensitized solar cells. *J. Mater. Chem. A* **2018**, *6*, 14518–14545. [CrossRef]
2. Hagfeldt, A.; Boschloo, G.; Sun, L.; Kloo, L.; Pettersson, H. Dye-Sensitized Solar Cells. *Chem. Rev.* **2010**, *110*, 6595–6663. [CrossRef] [PubMed]
3. Mahmood, A.; Hu, J.-Y.; Xiao, B.; Tang, A.; Wang, X.; Zhou, E. Recent progress in porphyrin-based materials for organic solar cells. *J. Mater. Chem. A* **2018**, *6*, 16769–16797. [CrossRef]
4. Yu, R.; Yao, H.; Hou, J. Recent Progress in Ternary Organic Solar Cells Based on Nonfullerene Acceptors. *Adv. Energy. Mater.* **2018**, *8*. [CrossRef]

5. Meng, L.; Zhang, Y.; Wan, X.; Li, C.; Zhang, X.; Wang, Y.; Ke, X.; Xiao, Z.; Ding, L.; Xia, R.; et al. Organic and solution-processed tandem solar cells with 17.3% efficiency. *Science* **2018**, *361*, 1094–1098. [CrossRef] [PubMed]

6. Lu, C.; Choi, I.T.; Kim, J.; Kim, H.K. Simple synthesis and molecular engineering of low-cost and star-shaped carbazole-based hole transporting materials for highly efficient perovskite solar cells. *J. Mater. Chem. A* **2017**, *5*, 20263–20276. [CrossRef]

7. Calió, L.; Kazim, S.; Grätzel, M.; Ahmad, S. Hole-Transport Materials for Perovskite Solar Cells. *Angew. Chem. Int. Ed.* **2016**, *55*, 14522–14545. [CrossRef]

8. Yang, S.; Fu, W.; Zhang, Z.; Chen, H.; Li, C.-Z. Recent advances in perovskite solar cells: Efficiency, stability and lead-free perovskite. *J. Mater. Chem. A* **2017**, *5*, 11462–11482. [CrossRef]

9. Freitag, M.; Teuscher, J.; Saygili, Y.; Zhang, X.; Giordano, F.; Liska, P.; Hua, J.; Zakeeruddin, S.M.; Moser, J.-E.; Grätzel, M.; et al. Dye-sensitized solar cells for efficient power generation under ambient lighting. *Nat. Photonics* **2017**, *11*, 372–378. [CrossRef]

10. Tsai, M.-C.; Wang, C.-L.; Chang, C.-W.; Hsu, C.-W.; Hsiao, Y.-H.; Liu, C.-L.; Wang, C.-C.; Lin, S.-Y.; Lin, C.-Y. A large, ultra-black, efficient and cost-effective dye-sensitized solar module approaching 12% overall efficiency under 1000 lux indoor light. *J. Mater. Chem. A* **2018**, *6*, 1995–2003. [CrossRef]

11. Oregan, B.; Gratzel, M. A Low-Cost, High-Efficiency Solar-Cell Based on Dye-Sensitized Colloidal Tio2 Films. *Nature* **1991**, *353*, 737–740. [CrossRef]

12. Kang, S.H.; Choi, I.T.; Kang, M.S.; Eom, Y.K.; Ju, M.J.; Hong, J.Y.; Kang, H.S.; Kim, H.K. Novel D-pi-A structured porphyrin dyes with diphenylamine derived electron-donating substituents for highly efficient dye-sensitized solar cells. *J. Mater. Chem. A* **2013**, *1*, 3977–3982. [CrossRef]

13. Eom, Y.K.; Kang, S.H.; Choi, I.T.; Yoo, Y.J.; Kim, J.H.; Kim, H.K. Significant light absorption enhancement by a single heterocyclic unit change in the pi-bridge moiety from thieno[3,2-b]benzothiophene to thieno[3,2-b]indole for high performance dye-sensitized and tandem solar cells. *J. Mater. Chem. A* **2017**, *5*, 2297–2308. [CrossRef]

14. Li, P.; Zhang, H.; Troisi, A. Systematic Study of the Effect of Auxiliary Acceptors in D–A′−π–A Sensitizers Used on Dye-Sensitized Solar Cells. *J. Phys. Chem. C* **2018**, *122*, 23890–23898. [CrossRef]

15. Han, L.; Islam, A.; Chen, H.; Malapaka, C.; Chiranjeevi, B.; Zhang, S.; Yang, X.; Yanagida, M. High-efficiency dye-sensitized solar cell with a novel co-adsorbent. *Energy Environ. Sci.* **2012**, *5*. [CrossRef]

16. Kakiage, K.; Aoyama, Y.; Yano, T.; Oya, K.; Fujisawa, J.; Hanaya, M. Highly-efficient dye-sensitized solar cells with collaborative sensitization by silyl-anchor and carboxy-anchor dyes. *Chem. Commun. (Camb.)* **2015**, *51*, 15894–15897. [CrossRef] [PubMed]

17. Nazeeruddin, M.K.; Péchy, P.; Grätzel, M. Efficient panchromatic sensitization of nanocrystalline TiO$_2$ films by a black dye based on a trithiocyanato–ruthenium complex. *Chem. Commun.* **1997**, 1705–1706. [CrossRef]

18. Aghazada, S.; Nazeeruddin, M. Ruthenium Complexes as Sensitizers in Dye-Sensitized Solar Cells. *Inorganics* **2018**, *6*. [CrossRef]

19. Li, X.; Zhang, X.; Hua, J.; Tian, H. Molecular engineering of organic sensitizers with o,p-dialkoxyphenyl-based bulky donors for highly efficient dye-sensitized solar cells. *Mol. Syst. Des. Eng.* **2017**, *2*, 98–122. [CrossRef]

20. Eom, Y.K.; Choi, I.T.; Kang, S.H.; Lee, J.; Kim, J.; Ju, M.J.; Kim, H.K. Thieno[3,2-b][1]benzothiophene Derivative as a New pi-Bridge Unit in D-pi-A Structural Organic Sensitizers with Over 10.47% Efficiency for Dye-Sensitized Solar Cells. *Adv. Energy. Mater.* **2015**, *5*, 1500300. [CrossRef]

21. Higashino, T.; Imahori, H. Porphyrins as excellent dyes for dye-sensitized solar cells: Recent developments and insights. *Dalton Trans.* **2015**, *44*, 448–463. [CrossRef] [PubMed]

22. Song, H.; Liu, Q.; Xie, Y. Porphyrin-sensitized solar cells: Systematic molecular optimization, coadsorption and cosensitization. *Chem. Commun.* **2018**, *54*, 1811–1824. [CrossRef] [PubMed]

23. Urbani, M.; Gratzel, M.; Nazeeruddin, M.K.; Torres, T. Meso-substituted porphyrins for dye-sensitized solar cells. *Chem. Rev.* **2014**, *114*, 12330–12396. [CrossRef] [PubMed]

24. Mathew, S.; Yella, A.; Gao, P.; Humphry-Baker, R.; Curchod, B.F.; Ashari-Astani, N.; Tavernelli, I.; Rothlisberger, U.; Nazeeruddin, M.K.; Gratzel, M. Dye-sensitized solar cells with 13% efficiency achieved through the molecular engineering of porphyrin sensitizers. *Nat. Chem.* **2014**, *6*, 242–247. [CrossRef] [PubMed]

25. Kang, S.H.; Jeong, M.J.; Eom, Y.K.; Choi, I.T.; Kwon, S.M.; Yoo, Y.; Kim, J.; Kwon, J.; Park, J.H.; Kim, H.K. Porphyrin Sensitizers with Donor Structural Engineering for Superior Performance Dye-Sensitized Solar Cells and Tandem Solar Cells for Water Splitting Applications. *Adv. Energy. Mater.* **2017**, *7*, 1602117. [CrossRef]

26. Wang, C.-L.; Hu, J.-Y.; Wu, C.-H.; Kuo, H.-H.; Chang, Y.-C.; Lan, Z.-J.; Wu, H.-P.; Wei-Guang Diau, E.; Lin, C.-Y. Highly efficient porphyrin-sensitized solar cells with enhanced light harvesting ability beyond 800 nm and efficiency exceeding 10%. *Energy Environ. Sci.* **2014**, *7*. [CrossRef]

27. Chen, Y.; Li, A.; Huang, Z.-H.; Wang, L.-N.; Kang, F. Porphyrin-Based Nanostructures for Photocatalytic Applications. *Nanomaterials* **2016**, *6*. [CrossRef] [PubMed]

28. Shiu, J.-W.; Chang, Y.-C.; Chan, C.-Y.; Wu, H.-P.; Hsu, H.-Y.; Wang, C.-L.; Lin, C.-Y.; Diau, E.W.-G. Panchromatic co-sensitization of porphyrin-sensitized solar cells to harvest near-infrared light beyond 900 nm. *J. Mater. Chem. A* **2015**, *3*, 1417–1420. [CrossRef]

29. Hill, J.P. Molecular Engineering Combined with Cosensitization Leads to Record Photovoltaic Efficiency for Non-ruthenium Solar Cells. *Angew. Chem. Int. Ed.* **2016**, *55*, 2976–2978. [CrossRef] [PubMed]

30. Zhang, L.; Cole, J.M. Dye aggregation in dye-sensitized solar cells. *J. Mater. Chem. A* **2017**, *5*, 19541–19559. [CrossRef]

31. Yella, A.; Lee, H.W.; Tsao, H.N.; Yi, C.; Chandiran, A.K.; Nazeeruddin, M.K.; Diau, E.W.; Yeh, C.Y.; Zakeeruddin, S.M.; Gratzel, M. Porphyrin-sensitized solar cells with cobalt (II/III)-based redox electrolyte exceed 12 percent efficiency. *Science* **2011**, *334*, 629–634. [CrossRef] [PubMed]

32. Cheng, Y.; Yang, G.; Jiang, H.; Zhao, S.; Liu, Q.; Xie, Y. Organic Sensitizers with Extended Conjugation Frameworks as Cosensitizers of Porphyrins for Developing Efficient Dye-Sensitized Solar Cells. *ACS Appl. Mater. Interfaces* **2018**. [CrossRef] [PubMed]

33. Krishna, J.V.S.; Krishna, N.V.; Chowdhury, T.H.; Singh, S.; Bedja, I.; Islam, A.; Giribabu, L. Kinetics of dye regeneration in liquid electrolyte unveils efficiency of 10.5% in dye-sensitized solar cells. *J. Mater. Chem C* **2018**, *6*, 11444–11456. [CrossRef]

34. Yella, A.; Mai, C.L.; Zakeeruddin, S.M.; Chang, S.N.; Hsieh, C.H.; Yeh, C.Y.; Gratzel, M. Molecular engineering of push-pull porphyrin dyes for highly efficient dye-sensitized solar cells: The role of benzene spacers. *Angew. Chem. Int. Ed. Engl.* **2014**, *53*, 2973–2977. [CrossRef] [PubMed]

35. Zhou, H.; Zhang, Y.; Mai, C.-K.; Seifter, J.; Nguyen, T.-Q.; Bazan, G.C.; Heeger, A.J. Solution-Processed pH-Neutral Conjugated Polyelectrolyte Improves Interfacial Contact in Organic Solar Cells. *ACS Nano* **2014**, *9*, 371–377. [CrossRef] [PubMed]

36. Liu, X.; Sun, Y.; Hsu, B.B.Y.; Lorbach, A.; Qi, L.; Heeger, A.J.; Bazan, G.C. Design and Properties of Intermediate-Sized Narrow Band-Gap Conjugated Molecules Relevant to Solution-Processed Organic Solar Cells. *J. Am. Chem. Soc.* **2014**, *136*, 5697–5708. [CrossRef] [PubMed]

37. Zheng, L.; Cao, Q.; Wang, J.; Chai, Z.; Cai, G.; Ma, Z.; Han, H.; Li, Q.; Li, Z.; Chen, H. Novel D–A$-\pi$–A-Type Organic Dyes Containing a Ladderlike Dithienocyclopentacarbazole Donor for Effective Dye-Sensitized Solar Cells. *ACS Omega* **2017**, *2*, 7048–7056. [CrossRef]

38. Zhang, M.; Yao, Z.; Yan, C.; Cai, Y.; Ren, Y.; Zhang, J.; Wang, P. Unraveling the Pivotal Impacts of Electron-Acceptors on Light Absorption and Carrier Photogeneration in Perylene Dye Sensitized Solar Cells. *ACS Photonics* **2014**, *1*, 710–717. [CrossRef]

39. Zhao, Y.; Truhlar, D.G. The M06 suite of density functionals for main group thermochemistry, thermochemical kinetics, noncovalent interactions, excited states, and transition elements: Two new functionals and systematic testing of four M06-class functionals and 12 other functionals. *Theor. Chem. Acc.* **2007**, *120*, 215–241. [CrossRef]

40. Hay, P.J.; Wadt, W.R. Ab initio effective core potentials for molecular calculations. Potentials for the transition metal atoms Sc to Hg. *J. Chem. Phys.* **1985**, *82*, 270–283. [CrossRef]

41. Hariharan, P.C.; Pople, J.A. The influence of polarization functions on molecular orbital hydrogenation energies. *Theor. Chim. Acta* **1973**, *28*, 213–222. [CrossRef]

42. Kang, M.S.; Choi, I.T.; Kim, Y.W.; You, B.S.; Kang, S.H.; Hong, J.Y.; Ju, M.J.; Kim, H.K. Novel D–π–A structured Zn(ii)–porphyrin dyes with bulky fluorenyl substituted electron donor moieties for dye-sensitized solar cells. *J. Mater. Chem. A* **2013**, *1*, 9848. [CrossRef]

43. Kang, M.S.; Kang, S.H.; Kim, S.G.; Choi, I.T.; Ryu, J.H.; Ju, M.J.; Cho, D.; Lee, J.Y.; Kim, H.K. Novel D–π–A structured Zn(ii)-porphyrin dyes containing a bis(3,3-dimethylfluorenyl)amine moiety for dye-sensitised solar cells. *Chem. Commun.* **2012**, *48*. [CrossRef] [PubMed]

44. Song, B.J.; Song, H.M.; Choi, I.T.; Kim, S.K.; Seo, K.D.; Kang, M.S.; Lee, M.J.; Cho, D.W.; Ju, M.J.; Kim, H.K. A Desirable Hole-Conducting Coadsorbent for Highly Efficient Dye-Sensitized Solar Cells through an Organic Redox Cascade Strategy. *Chem. Eur. J.* **2011**, *17*, 11115–11121. [CrossRef] [PubMed]

45. Lee, M.J.; Seo, K.D.; Song, H.M.; Kang, M.S.; Eom, Y.K.; Kang, H.S.; Kim, H.K. Novel D-pi-A system based on zinc-porphyrin derivatives for highly efficient dye-sensitised solar cells. *Tetrahedron Lett.* **2011**, *52*, 3879–3882. [CrossRef]

46. Song, H.M.; Seo, K.D.; Kang, M.S.; Choi, I.T.; Kim, S.K.; Eom, Y.K.; Ryu, J.H.; Ju, M.J.; Kim, H.K. A simple triaryl amine-based dual functioned co-adsorbent for highly efficient dye-sensitized solar cells. *J. Mater. Chem.* **2012**, *22*, 3786–3794. [CrossRef]

47. Yum, J.-H.; Baranoff, E.; Kessler, F.; Moehl, T.; Ahmad, S.; Bessho, T.; Marchioro, A.; Ghadiri, E.; Moser, J.-E.; Yi, C.; et al. A cobalt complex redox shuttle for dye-sensitized solar cells with high open-circuit potentials. *Nat. Commun.* **2012**, *3*. [CrossRef]